First-principles studies of Au-induced nanowires on Ge(001)

S. Sauer, F. Fuchs, and F. Bechstedt
Institut für Festkörpertheorie und -optik, European Theoretical Spectroscopy Facility (ETSF), Friedrich-Schiller-Universität, Max-Wien-Platz 1, 07743 Jena, Germany

C. Blumenstein and J. Schäfer
Physikalisches Institut, Universität Würzburg, 97074 Würzburg, Germany
(Received 9 November 2009; published 12 February 2010)

The geometry, stability, and electronic properties of Au-induced quantum wire structures on Ge(001) surfaces with $c(8\times2)$ and $p(4\times2)$ translational symmetry are investigated using total-energy and electronic-structure calculations based on density-functional theory in local and semilocal approximations for exchange and correlation. About 150 candidates for surface structures and their various possible modifications with varying bonding geometry and stoichiometry have been studied. The most favorable structures are classified in the four classes of gold chains on the dimerized Ge(001) surface, chains due to the replacement of Ge dimers by Au or mixed Au-Ge dimers, bridged dimer-row structures, and Au/Ge wire structures stabilized by Au-covered low-index facets. The relaxed surfaces are evaluated with respect to their total energy, scanning tunneling microscopy (STM) signatures, and band structures in comparison to the available experimental data. We identify several features of energetically favorable models which agree with measurements. However, no model completely fulfills the combinations of low formation energy, agreement with experimental STM images, and the occurrence of a one-dimensional parabolic band crossing the Fermi level.

DOI: 10.1103/PhysRevB.81.075412 PACS number(s): 68.35.bg, 68.37.Ef, 68.43.Fg

I. INTRODUCTION

One-dimensional (1D) electronic systems attract enormous interest because of their exotic electronic properties. In particular, a charge-density wave (CDW) can occur in quasi-1D systems,[1] which relates to the specific Fermi-surface topology. A more unusual phenomenon is the Luttinger liquid state,[2] which can exhibit features such as separation of the spin and charge degrees of freedom, as well as suppressed spectral weight at the Fermi level at low temperature. Experimental studies that search for signatures of the Luttinger liquid in various materials are ongoing, as representatives are rare. In the past, realizations have been found, e.g., in crystalline 1D-bonded solids.[3,4]

A class of very promising materials is arrays of metal-induced atomic wires on group-IV semiconductor substrates. They can be grown by self-assembly at elevated temperature. The general idea is that a substrate with an energy gap ensures a decoupling of the wires, although the actual interchain interaction will critically depend on their lateral extent and the orbital overlap of neighboring chains. Examples of atomic nanowires are Au-induced chains on Si(111)-derived high-index faces, such as (553) and (557),[5–7] as well as In chains on In/Si(111) in the (4×1) high-temperature phase[8] and the (8×2) low-temperature phase.[9] Phase transitions observed in these systems are being discussed within pictures like a CDW or structurally driven transitions, respectively.[10]

In recent years, atomic nanowires have also been successfully grown on Ge(001). Pt adatoms lead to well separated chains.[11–13] Moreover, also Au can induce nanowires with the same spacing. Chainlike growth of Au on Ge(001) was observed with scanning tunneling microscopy (STM) in a wide range of coverages.[14] However, only in recent reports long-range order in $c(8\times2)$ symmetry was achieved.[15,16] These Au-induced chains grow in the $\langle110\rangle$ direction and are separated by approximately 1.6 nm, i.e., by four Ge(001) 1×1 lattice constants of $a_0/\sqrt{2}=4.0$ Å.[15,17] Interestingly, while there is indication that the Pt nanowires are almost insulating,[12,13] the Au chains exhibit significant metallic conductivity, as seen in STM and photoemission spectroscopy.[15]

However, not only the exact coverage but also the details of the wire structure (e.g., corrugation, dimerization, and buckling) and the nature of the reconstruction are under discussion. The atomic geometry of the Au-induced chain structures is currently unknown from both an experimental and theoretical point of view. Wang *et al.*[14] suggested that the white and gray chains in their STM images can be explained by Au-Au and Au-Ge dimer rows, respectively. Based on their STM images other authors,[17] however, proposed a giant missing-row (GMR) reconstruction with Au-decorated microfacets of the {111} type. Both suggestions, until today, have not yet been evaluated by corresponding theoretical modeling.

In the last years, it has been demonstrated that total-energy optimizations of covered surfaces in the framework of density-functional theory (DFT) represent an excellent tool to explore the atomic arrangements behind the measured STM images and other spectroscopic quantities. This was relatively easy for the double In-In zigzag chains at the high-temperature In/Si(111) 4×1 surface.[18,19] Also, studying the low-temperature In/Si(111) 8×2 phase and the driving forces for the phase transition, DFT calculations[20,21] suggest a specific atomic geometry, despite an ongoing controversy.[22] Such investigations have driven the scientific discussion by finding alternative explanations for experimental observations, as shown for the Au/Si(557) surface.[23] A screening of more than 20 possible structural models[24] together with the knowledge of surface stability with orientation and recon-

TABLE I. Cubic lattice constant a_0 (in Å) and cohesive energy E_{coh} per atom (in eV) calculated within DFT-LDA and DFT-GGA (see text). The energy value in parentheses takes the spin polarization of the free atom into account. For comparison experimental values (second line) are listed (Ref. 33).

	Au		Ge	
Parameter	LDA	GGA	LDA	GGA
a_0	4.06	4.17	5.63	5.77
Expt.	4.08		5.66	
E_{coh}	4.40 (4.28)	3.20 (3.04)	5.14 (4.63)	4.53 (3.82)
Expt.	3.81		3.85	

struction lead to the widely accepted tetramer-dimer-chain (TDC) model for nanowire arrays on the Pt/Ge(001) 4×2 surface.[13]

In order to explore the atomic geometry of the Au-induced nanowires on a Au/Ge(001) surface, in this paper we study a variety of overlayer structures by means of total-energy and electronic-structure calculations. The computational methods are described in Sec. II. The model structures and the accompanying STM images are presented in Secs. III–V for the Au-chain and dimer-row models, the bridging dimer (BD)-row models, and the models including deep trenches. Finally, in Sec. VI a summary and conclusions are given.

II. COMPUTATIONAL METHODS

A. Density-functional-theory approach

The total energies, the optimized atomic geometries, and the electronic structures are calculated within DFT as implemented in the Vienna *ab initio* simulation package (VASP).[25,26] The pseudopotentials and wave functions are generated within the projector-augmented wave method[27] with the valence electron configurations $3d^{10}4s^24p^2$ (Ge) and $5d^{10}6s^1$ (Au). According to our test calculations, a plane-wave cutoff of 29.4 Ry is sufficient for the treatment of the Au metal and the semicore Ge $3d$ electrons. It is significantly larger than in the case of clean Ge surfaces[28] or the Pt/Ge(001) system.[24] Since usually only surface unit cells with an even number of Au atoms are studied, most of the calculations do not account for spin polarization. The choice of the exchange-correlation (XC) functional deserves special attention. In this paper, the majority of presented results is obtained using a semilocal generalized gradient approximation (GGA).[29,30] For the purpose of comparison, we repeated the calculations in the framework of the local-density approximation (LDA) for XC.[31] Because of the non-negligible differences for the surface energies results in both approximations are given. For the geometrical properties, however, only the results obtained within GGA are presented since their principal changes with respect to the LDA results are small. The most important difference is a general shortening of the bond lengths which can be accounted for mostly by a simple rescaling according to change in the bulk Ge lattice constant between 0.5% underestimation (LDA) or 1.9% overestimation (GGA) in comparison to experimental data.

The **k**-space integrations required for the evaluation of total energies and electron densities are replaced by summations over Monkhorst-Pack (MP) type **k** points.[32] In order to minimize the total energies with respect to the atomic positions and to obtain the equilibrium coordinates, the positions are relaxed until the Hellmann-Feynman forces are less than 10 meV/Å. The results for bulk Ge and Au crystallizing in diamond or fcc structure are given in Table I. We find excellent agreement with other computed lattice constants and cohesive energies.[24,34,35] In comparison to the experimental data we observe the typical overbinding (underbinding) for LDA (GGA) treatment of XC. Thereby LDA gives the best agreement for the lattice constants while GGA (including spin polarization of the free atom) gives almost the correct cohesive energy of Ge. Unfortunately, the deviations for Au are much larger (about −20%). This huge deviation may introduce a significant underestimation of the binding energy of Au atoms to the Ge surface, especially if surface formation energies for adsorbate systems with varying number of Au atoms (see below) are compared. It may influence the energetic ordering of surface geometry models with not too many Au atoms. In order to illustrate the influence of XC when comparing structures with varying number of Au atoms, in addition to the GGA energy values we list the LDA ones. The two approaches may lead to completely different surface formation energies since the difference of the E_{coh} values in GGA and LDA for Au amounts to 1.2 eV/atom. On the other hand, the corresponding difference is with −0.4 eV/atom much smaller for Ge but has a different sign. In any case due to the significant influence of the XC treatment the resulting surface formation energies have to be interpreted carefully. In order to clarify more the influence of the XC functional we have also tested the PBE one.[36] It practically leads to the same atomic distances as GGA but to slightly increased total energies (reduced cohesive energies). However, the relative formation energies remain also almost the same as computed for the most important nanowire models. Because of the similarities we present only results for GGA in comparison to LDA.

B. Surface modeling

Both clean and gold covered Ge(001) surfaces are simulated by repeated asymmetric slabs with eight Ge layers and a vacuum thickness of 16–20 Å. Five of the eight atomic layers are allowed to relax. The bottom side of each slab with

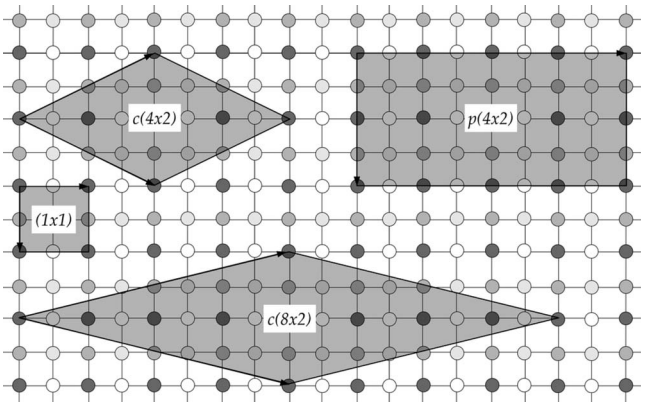

FIG. 1. Two-dimensional surface unit cells of the Ge(001) surface used. Four atomic layers are represented. The gray scale of the atoms indicates atoms in different layers. The edge of a 1×1 cell is given by $a_0/\sqrt{2}\approx4$ Å.

fixed atomic positions is saturated by hydrogen (H) atoms. The surface translational symmetry is forced to be $c(8\times2)$ in agreement with experimental findings[14,15] or $p(4\times2)$ as suggested alternatively[17] (see Fig. 1). We mostly focus on a coverage of about 0.5 monolayers as determined experimentally,[15] i.e., four Au atoms in a $c(8\times2)/p(4\times2)$ cell. However, also other—especially increased—coverages are studied to account for other surface preparations.[14] The Au-induced wires are assumed to be parallel to the [110] direction. The **k**-space summations are performed using MP meshes of $3\times3\times1$ for $c(8\times2)$ cells and $2\times4\times1$ for $p(4\times2)$ cells.

A variety of surface atomic geometries with varying numbers N_{Au} of Au atoms and N_{Ge} of Ge atoms has to be evaluated energetically. This suggests to use Planck's grand canonical thermodynamic potential. More precisely, we compare surface formation energies (per surface unit cell of a given slab) of the form

$$\Omega_{\mathrm{f}} = E_{\mathrm{slab}}(N_{\mathrm{Ge}},N_{\mathrm{Au}},N_{\mathrm{H}}) - \mu_{\mathrm{Ge}}N_{\mathrm{Ge}} - \mu_{\mathrm{Au}}N_{\mathrm{Au}} - \mu_{\mathrm{H}}N_{\mathrm{H}} \quad (1)$$

with E_{slab} as the total energy of the slab containing N_{Ge} $(N_{\mathrm{Au}},N_{\mathrm{H}})$ Ge (Au, H) atoms. There may be a particle exchange with certain reservoirs described by the corresponding chemical potentials μ_{Ge}, μ_{Au}, and μ_{H}. Because of the bulk Ge as substrate we fix $\mu_{\mathrm{Ge}}=-E_{\mathrm{coh}}$ with the theoretical value $E_{\mathrm{coh}}=4.53$ eV (GGA) or 5.14 eV (LDA). The chemical potential μ_{Au} of the gold reservoir varies according to

$$\mu_{\mathrm{Au}} = \mu_{\mathrm{Au}}^{\mathrm{bulk}} + \Delta\mu_{\mathrm{Au}} \quad (2)$$

with $\mu_{\mathrm{Au}}^{\mathrm{bulk}}=-E_{\mathrm{coh}}$ and hence $\mu_{\mathrm{Au}}^{\mathrm{bulk}}=-3.20$ eV (GGA) or $\mu_{\mathrm{Au}}^{\mathrm{bulk}}=-4.40$ eV (LDA), and $-\infty<\Delta\mu_{\mathrm{Au}}<0$ depending on the preparation conditions. The slab approximation contains two surfaces, a Au-covered and a H-passivated one (we are not interested in the latter one). Therefore, instead of Eq. (1) we only study a relative formation energy of the Au-modified surfaces

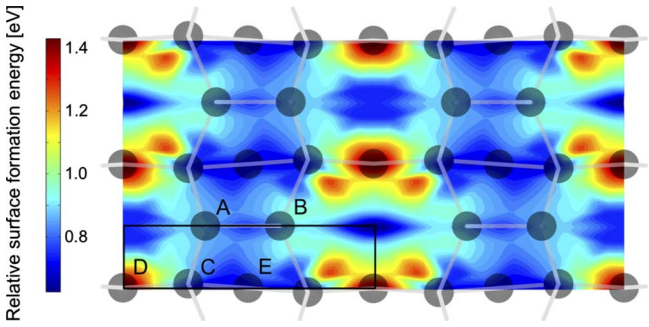

FIG. 2. (Color online) Relative surface formation energy of an Au atom on a dimerized Ge(001) $p(4\times2)$ surface in DFT-GGA for $\mu_{\mathrm{Au}}=\mu_{\mathrm{Au}}^{\mathrm{bulk}}$. The irreducible part of the unit cell and important substitution sites are indicated by solid lines and capital letters, respectively.

$$\Delta\Omega_{\mathrm{f}} = E_{\mathrm{slab}}(N_{\mathrm{Ge}},N_{\mathrm{Au}},N_{\mathrm{H}}) - E_{\mathrm{slab}}(N_{\mathrm{Ge}}^{\mathrm{clean}},0,N_{\mathrm{H}}) - \mu_{\mathrm{Ge}}(N_{\mathrm{Ge}} - N_{\mathrm{Ge}}^{\mathrm{clean}}) - \mu_{\mathrm{Au}}N_{\mathrm{Au}} \quad (3)$$

with respect to the energy of the corresponding slab of the clean Ge surface with $N_{\mathrm{Ge}}^{\mathrm{clean}}$ Ge atoms in the slab. We refer to the clean, dimerized, and relaxed Ge(001) surface with the $c(4\times2)$ ground-state reconstruction. A slab with a $c(8\times2)$ lateral unit cell contains $N_{\mathrm{Ge}}^{\mathrm{clean}}=64$ and $N_{\mathrm{H}}=16$ atoms. Within the DFT-GGA framework the slab energy amounts to $E_{\mathrm{slab}}(N_{\mathrm{Ge}}^{\mathrm{clean}},0,N_{\mathrm{H}})=-332.52$ eV.

Important information about the adsorption of Au atoms in general can be derived by studying an isolated Au atom on top of the clean, dimerized Ge(001) surface. Thereby, the lateral coordinates x,y of the test Au atom are fixed while its vertical coordinate z and the position of the surface Ge atoms are allowed to relax. The DFT-GGA results for the formation energy [Eq. (3)] with one Au atom on a $p(4\times2)$ surface unit cell, i.e., the negative of the gold adsorption energy, are plotted in Fig. 2 for a bulk Au reservoir with $\mu_{\mathrm{Au}}=-E_{\mathrm{coh}}$. The positive surface formation energy for all lateral positions indicates that even under extremely Au-rich preparation conditions ($\Delta\mu_{\mathrm{Au}}=0$) the adsorption of an isolated Au atom is unstable. The position with the lowest formation energy is found between two buckled Ge dimers in adjacent dimer rows. Other relatively stable positions are observed along the dimer rows, especially on top or in between the dimers.

The latter finding may also be interpreted as a tendency for substitution of Ge atoms. The exchange of Ge atoms at the positions A, B, C, D, and E with Au atoms, i.e., $N_{\mathrm{Ge}}-N_{\mathrm{Ge}}^{\mathrm{clean}}=-1$ and $N_{\mathrm{Au}}=1$, leads to relative formation energies [Eq. (3)] of $\Delta\Omega_{\mathrm{f}}=0.17$, -0.06, 0.50, 0.93, and 0.46 eV for $\mu_{\mathrm{Au}}=\mu_{\mathrm{Au}}^{\mathrm{bulk}}$. Indeed, under extremely Au-rich preparation conditions the replacement of top Ge dimer atoms is favorable, only at the position of the down-buckled dimer atom B. A possible explanation of this finding is that Au atoms prefer to form Ge-Au bonds and to be almost threefold coordinated. However, the tendency seems to be much weaker pronounced as in the case of Ge substitution by Pt atoms. For Pt, similar calculations[24] lead to larger energy gains $-\Delta\Omega_{\mathrm{f}}$. Consequently, the most favorable tetramer-dimer-chain model for Pt adsorption gives an $\Delta\Omega_{\mathrm{f}}$ of -2 eV per $p(4\times2)$ cell while

in the case of Au the corresponding energy amounts to 0.69 eV (in an equivalent geometry). The main reason is the increased number of electrons per 5*d* metal atom. The Au atoms show a stronger tendency to keep the 5*d* shell intact with the consequence that they prefer a threefold coordination instead of the fourfold coordination observed for Pt atoms, e.g., in the TDC reconstruction. Another reason might be given by the different electron transfers. In the Pt case the dangling bonds belonging to the Ge atoms adjacent to Pt atoms are almost empty.[24] In the Au case there is no need for electron transfer and the Ge dangling bonds get reconstructed to gain energy but simultaneously also loose energy due to the induced local strain. So obviously, going from Pt→Au asks for completely different bonding configurations.

C. STM images

The eigenvalues and eigenfunctions of the Kohn-Sham equation of the DFT (Refs. 25 and 26) are not only used to calculate the electronic properties such as electron densities and total densities of states but also to derive energy-resolved local densities of states (LDOS) $\rho(\mathbf{x},\varepsilon)$. They allow to compute the bias dependence of the tunnel current $I=I(V_T)$ within the Tersoff-Hamann approach,[37]

$$I \sim \int_{\varepsilon_F}^{\varepsilon_F+eV_T} d\varepsilon \rho(\mathbf{x},\varepsilon) \tag{4}$$

with $\mathbf{x}$ as the position of the tip and ε_F as the Fermi energy of the system.

Since the experimental STM studies[14,15,17] are usually performed within the constant-current mode, all images in this paper are calculated to mimic this. Starting point is expression (4) for the tunnel current. However, in contrast to the calculation of the STM images within the constant-height mode, the finite extent of the tunnel tip has to be taken into account. In our approach we simulate the finite tip by a Gaussian smoothening of the LDOS $\rho(\mathbf{x},\varepsilon)$ with a Gaussian of 2.35 Å full width half maximum.[38]

III. GOLD CHAINS AND DIMER ROWS

Since the STM images[15] indicate nanowires which are laterally confined to the ultimate limit of single atom dimension and are strictly separated from their neighbors, a first modeling may start from linear or zigzag Au chains such as presented in Fig. 3. Varying the surface coverage with Au atoms Θ one may construct different structures of parallel chains in a distance of almost 16 Å. Linear chains ($\Theta=0.25$) and zigzag chains ($\Theta=0.50$) between dimer rows (geometries not shown in Fig. 3) lead to formation energies $\Delta\Omega_f=0.76$ or 2.89 eV in DFT-GGA. Therefore these models seem to be energetically unfavorable, probably due to too much tensilely or compressively strained Au-Au bonds. The bond-length values are 4.08 or 2.71 Å in DFT-GGA, which have to be compared to a bulk value of 2.94 Å. More compact zigzag chains as in the GC3 model [Fig. 3(c)] give rise to much smaller formation energies $\Delta\Omega_f$ [Eq. (3)] even for $\mu_{Au}=\mu_{Au}^{bulk}$ (cf. Table II). Here, the Au-Au distances are also rather small with 2.71 Å, leading to a much larger interaction between the Au atoms compared to the other gold chain (GC) models.

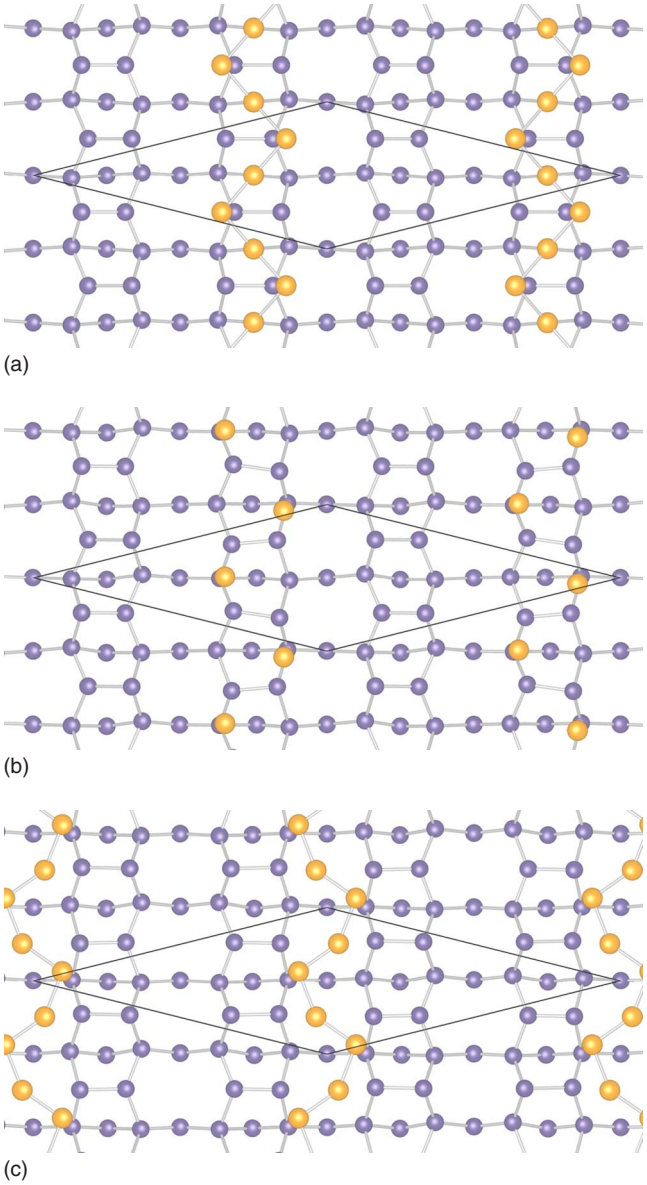

FIG. 3. (Color online) Top view on zigzag Au chains on a dimerized Ge(001) surface. The used $c(8\times2)$ unit cell is indicated. The Au coverage varies between (a) $\Theta=0.50$, (b) $\Theta=0.25$, and (c) $\Theta=0.50$.

More plausible are zigzag Au chains, i.e., GC models, on top of dimer rows as GC1 and GC2 in Fig. 3 with the relative formation energy $\Delta\Omega_f$ in Table II. Nevertheless, they are less favorable independent of the used XC functional compared to the GC3 geometry. The reason may be the strain induced in the underlying dimer rows. We studied 15 additional structures (not shown here), being variations and combinations of the three chain models GC1, GC2, and GC3 even for different coverages ($\Theta=0.375$). They all, however, were found to require larger formation energies $\Delta\Omega_f$.

The energetically most favorable models in our studies were found among those with a substitution of Ge dimer

TABLE II. Relative formation energies $\Delta\Omega_f$ in electron volt per unit cell of chain and dimer-row models in Figs. 3 and 4 for the Au/Ge(001) $c(8\times2)$ surface in GGA and LDA. The Au coverage Θ is given. Negative values of Θ_{Ge} indicate the reduction in Ge atoms in the surface in units of a monolayer. The chemical potential of Au is fixed at its bulk value.

	GC1	GC2	GC3	HD1	HD2	AD	AD/HD
Θ	0.50	0.25	0.50	0.25	0.25	0.50	0.75
Θ_{Ge}	0	0	0	−0.25	−0.25	−0.50	−0.75
$\Delta\Omega_f^{GGA}$	2.12	1.33	0.65	−0.10	0.00	**−0.72**	−0.70
$\Delta\Omega_f^{LDA}$	3.33	2.05	1.47	**0.30**	0.45	0.33	0.81

atoms by Au atoms and hence the formation of Ge-Au heterodimers (HD) and Au-Au homodimers (AD) in the dimer rows of the former clean Ge(001) surface. The resulting chain structures are depicted in Fig. 4. The configurations feature Au coverages between $\Theta=0.25,\ldots,0.75$, and, because only exchange reactions have been considered, corresponding Ge coverages of $\Theta_{Ge}=-0.25\cdots-0.75$. The formation energies of the resulting geometries are also listed in Table II. They show that the formation of homodimer and heterodimer is indeed energetically more favorable than the formation of on-top Au chains. The buckled Ge homodimers are less influenced by the presence of gold. The heterodimers can be unbuckled as in HD1 [Fig. 4(a)] or buckled as in HD2 [Fig. 4(b)] with a Ge atom in the upper position and a dimer tilt angle of 12.2°. The bond length of the Au dimer is 3.02 Å, similar to the atomic distance in bulk Au. The bond length of the heterodimer is shorter with 2.57 Å (HD1) and 2.53 Å (HD2). These values are comparable to that of buckled Ge-Ge dimer on the clean Ge(001) surface (2.57 Å, tilt angle 19.5°).

According to the GGA surface formation energies the AD model is more favorable than the models HD1 and HD2 (cf. Table II). Since the energy gain results solely from the Au adsorption at the Ge dimer chain it is just consequent to investigate the effects of Au adsorption on the remaining Ge dimer rows. Replacing the respective Ge dimers in the AD surface by Au homodimers, the formation energy is further lowered to $\Delta\Omega_f=-1.22$ eV in DFT-GGA under the extremely Au-rich preparation conditions $\mu_{Au}=\mu_{Au}^{bulk}$. Thereby the coverage is increased to $\Theta=1.00$. The resulting wire system, however, possesses only an 8 Å spacing between the nanowires which is in marked contrast to the experimental findings. A compromise between energy gain and wire-wire distance is the mixed AD/HD model in Fig. 4(d), originally postulated by Wang *et al.*,[14] with a coverage of $\Theta=0.75$. Its formation energy, however, being $\Delta\Omega_f=-0.70$ eV in DFT-GGA falls very close to that of the original AD model (Table II).

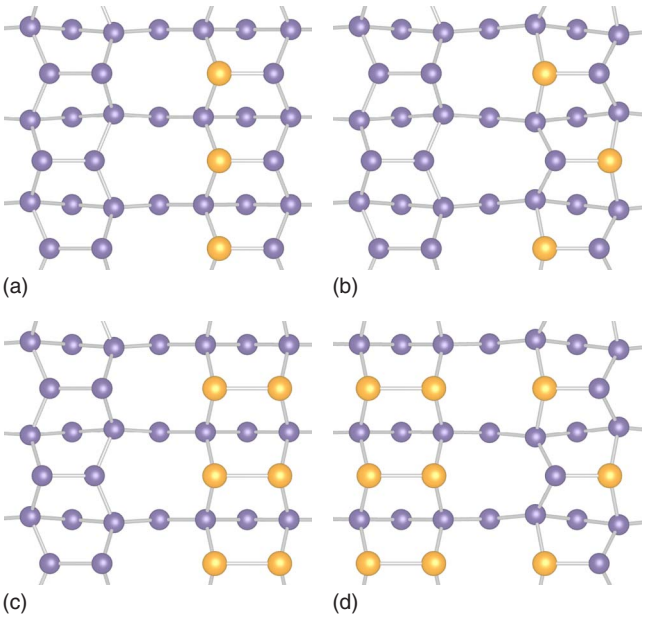

FIG. 4. (Color online) Top view on dimer rows with Au-Au ADs and Ge-Au HDs. The Au coverages vary between $\Theta=0.25$ and $\Theta=0.75$.

We can only speculate why the energetically most favorable AD structure with wires in a distance of 8 Å does not occur at the surfaces prepared in the experiments.[14,15,17] One explanation might be the influence of the XC functional on the surface formation energies. In fact, the AD structure turns out to be unstable judged upon the DFT-LDA result of $\Delta\Omega_f=0.33$ eV. Other explanations could be kinetic effects and diffusion barriers and, hence, the appearance of nonequilibrium geometries in the surface preparation.

In order to examine the possible occurrence of the dimer-row models, we have also calculated their STM signatures. Figure 5 shows the calculated constant-current mode STM images for the AD model [Fig. 4(c)] and the AD/HD geometry [Fig. 4(d)]. The tunnel bias voltage $|V_T|=1$ V is chosen to be somewhat below the typical voltages used in the experiments in order to account for the gap underestimation in the Kohn-Sham theory.[39] The prefactor of the tunnel current [Eq. (4)] contains a charge density that has been chosen to be $n_T=2e/\text{Å}^3$ $(0.5e/\text{Å}^3)$ for negative (positive) bias.

For both the AD and AD/HD models the tunneling-current images in Fig. 5 clearly exhibit a distance of about 16 Å between the nanowires as observed experimentally for both occupied and empty states.[14,15,17] They show elevated zigzag chains with varying width, which are generated by buckled Ge homodimers for the AD model or Ge-Au heterodimers for the AD/HD model. The Au homodimers are practically invisible for the STM (only weakly for positive bias). For the AD model the most pronounced STM features (bright spots) are the filled *s*-like dangling bond D_{up} for negative bias and empty p_z-like dangling bond D_{down} for positive bias.[28,40] In the case of the AD/HD model the role of the buckled Ge

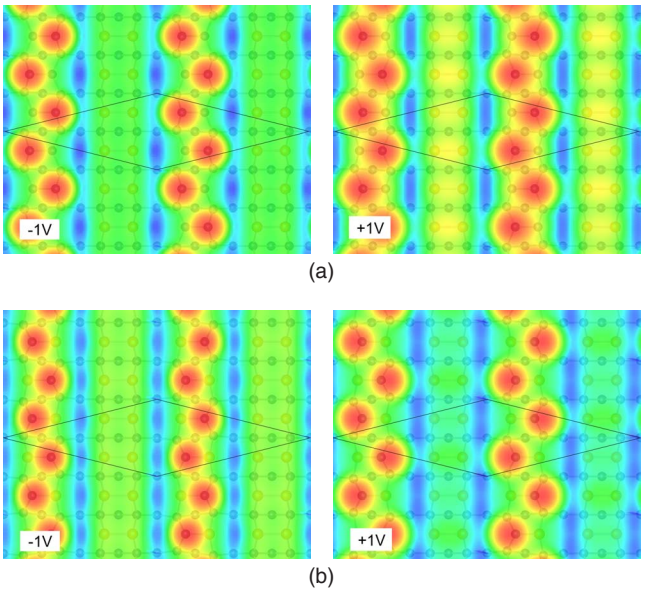

FIG. 5. (Color online) STM images for energetically favored dimer-row structures: (a) AD [Fig. 4(c)] and (b) AD/HD [Fig. 4(d)]. Left (right) panels are computed for occupied (empty) states. Bright/red regions describe protrusions while dark/blue areas indicate deep corrugations. The circles in the background refer to the atomic positions. Dotted lines illustrate a $c(8\times2)$ unit cell.

dimers is taken over by the buckled Au-Ge heterodimers. However, only the slightly elevated Ge atoms are visible in the STM images for negative and positive tunnel bias V_T. Therefore, in contrast to the AD model there is no phase shift between the occupied and unoccupied STM images. The trenches between the zigzag chains are given by Au homodimers in both models, in contrast to the interpretation of Wang *et al.*[14] However, these trenches are rather flat. The Au homodimers are about 0.4 (0.3) Å below the dimers in the adjacent rows in the AD (AD/HD) model. In the calculated STM images this height difference appears larger with values between 1 and 1.5 Å (depending on the tunneling voltage and current) since the local density of states close to the Fermi level is surprisingly lower at the Au dimer rows in comparison to the Ge dimer or Ge-Au heterodimer row, in contrast to the claims by Wang *et al.*[14] Unfortunately, the dimer-row models AD and AD/HR cannot explain the details of the observations of Schäfer *et al.*[15] and van Houselt *et al.*,[17] where especially larger corrugations and depths of the trenches have been observed.

IV. BRIDGING DIMER ROWS

The experimental STM results[15,17] suggest to construct models with deeper trenches. One possibility is to bridge each second trench. This gives rise to nanowires [cf., e.g., Fig. 6(a)] with a basis width of about 16 Å, which, therefore, easily explains the observed wire-wire distance of 16 Å, in contrast to the dimer-row models, where in principle also distances of 8 Å are plausible. There is another advantage. As indicated in the side view of Fig. 6(a), the wires along the [110] direction on the (001) surface now

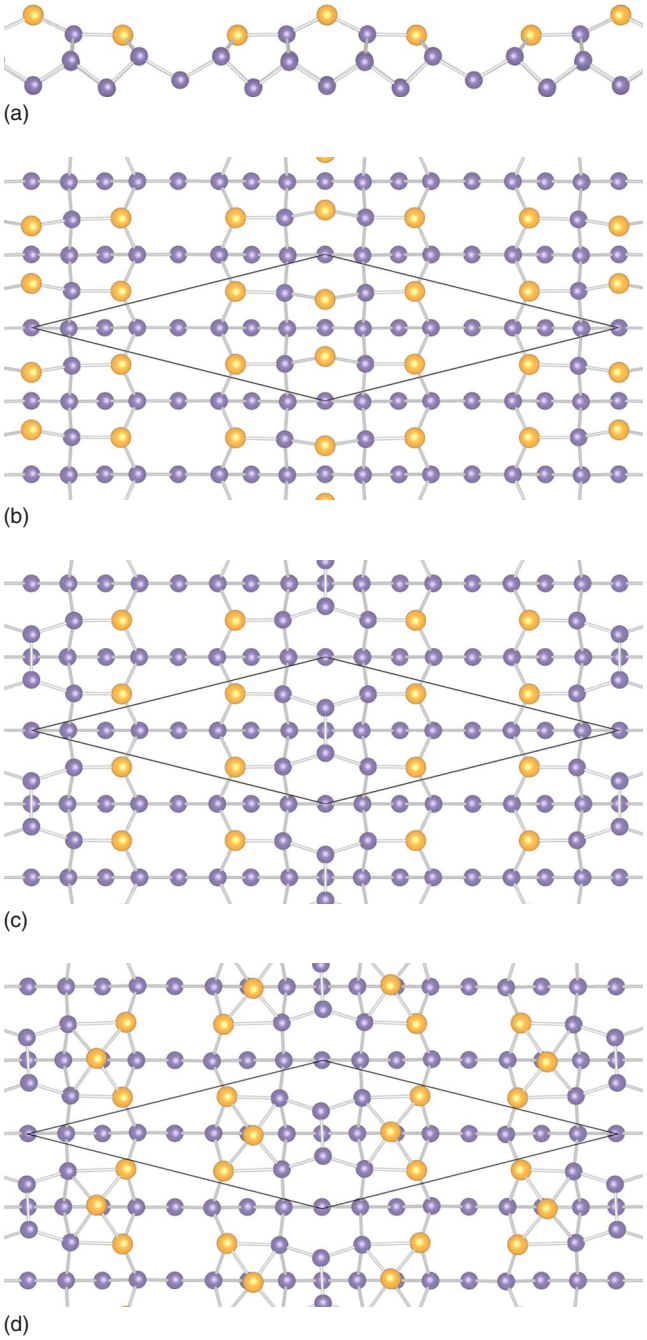

FIG. 6. (Color online) Stick-and-ball models for BD models: (a) and (b) Au-BD with Au homodimers, (c) Ge-BD with Ge dimers, and (d) EBD with Ge dimers and additional Au atoms stabilizing wire facets. The Au coverage varies between $\Theta=0.50$ and $\Theta=0.75$. The solid lines describe a $c(8\times2)$ unit cell.

possess facets with $[1\bar{1}4]$ and $[\bar{1}14]$ orientations. These orientations are known to lead to stable Ge surfaces.[41] Total-energy calculations also have shown that, e.g., {113} surfaces are more stable than {001} surfaces.[42] BDs could be Ge and Au homodimers as well as Au-Ge heterodimers. However, our calculations showed that models with bridging heterodimers are less stable than those with homodimers.

For that reason, only models with Au or Ge dimers, Au-BD and Ge-BD, are presented in Figs. 6(a)–6(c). They

TABLE III. Relative formation energies $\Delta\Omega_f$ in electron volt per unit cell of bridging dimer and giant missing-row models in Figs. 6 and 8 for the Au/Ge(001) $c(8\times2)/p(4\times2)$ surface in GGA and LDA. The Au coverage Θ is given. Negative values of Θ_{Ge} indicate the reduction in Ge atoms in the surface in units of a monolayer. The chemical potential of Au is fixed at its bulk value. For comparison the TDC model is also listed.

	Au-BD	Ge-BD	EBD	GMR	MGMR	ATSGR	TDC
Θ	0.75	0.50	0.75	1.00	0.50	0.75	0.25
Θ_{Ge}	−0.50	−0.25	−0.25	1.50	2.25	2.00	−0.25
$\Delta\Omega_f^{GGA}$	−0.52	−0.40	**−0.66**	1.48	0.93	**−0.44**	0.69
$\Delta\Omega_f^{LDA}$	0.72	0.08	**0.02**	3.41	1.77	0.21	0.90

are rather stable (cf. Table III) even for extremely Au-rich preparation conditions. The bridging dimers show bond lengths of 3.19 Å (Au-Au) and 2.50 Å (Ge-Ge) close to values of the bulk bond lengths. In contrast to the clean surface the bridging Ge homodimers are not buckled. Additional Au atoms [Fig. 6(d)] further lower the formation energy as demonstrated for an extended Ge bridging dimer (EBD) model in Table III. In this model the three Au atoms in each $c(8\times2)$ cell on the $[1\bar{1}4]$ and $[\bar{1}14]$ facets seem to form a trimer as observed for Au adsorbed on the Ge(111) surface.[43,44]

STM images (constant-current mode) computed for the three most stable bridging dimer models Au-BD, Ge-BD, and EBD are presented in Fig. 7. Unbuckled bridging dimers give rise to similar STM images independent of the chemical nature, Au or Ge, of the dimer atoms. There are only small changes due to the contributing different orbitals and number of atoms. The calculated images show alternating wires and trenches with a distance of 16 Å. Each individual chain link represented by a bridging dimer is visible in the STM images for both occupied and empty states. This result is somewhat in contrast to the experimental findings, where no isolated atoms or dimers could be identified. In addition, complex features as the "butterflylike" structures in the Au-BD images for negative bias voltage have not been observed experimentally. For the EBD model, the additional Au atom at each facet leads to drastic changes of the STM images [cf. Fig. 7(c)], especially for a positive tunnel bias. Then, the Au atoms give rise to isolated features. They may be related to the "grains" observed on the wires that tend to lead to a larger superstructure with a period of 32 Å in wire direction.[15,45]

V. WIRES SEPARATED BY DEEP TRENCHES

From the height profiles of their STM images, van Houselt *et al.*[17] concluded a surface corrugation of not less than 6 Å. Such deep trenches between the nanostripes in $[\bar{1}10]$ direction separated 16 Å apart should have $\{11n\}$ facets on both sides. Since $n=4$ only gives rise to a depth of about 1 Å, they deduced $n=1$ and hence Au-induced nanostripes due to alternating (111) and $(\bar{1}\bar{1}1)$ facets. The facets are further stabilized by Au atoms, which exhibit a $(\sqrt{3}\times\sqrt{3})R30°$ reconstruction similar to the Au-induced reconstruction of Ge(111).[43,44] The top of the nanostripes is formed by a Ge dimer row. The authors denoted their model as GMR model.[17]

In the original paper[17] no translational symmetry is given. According to Fig. 3 in that paper, the unit cell is suggested to show a ×6 periodicity (i.e., 24 Å) in wire direction and an extend of 16 Å in the perpendicular direction. However, a 6×4 reconstruction has not been observed experimentally. We therefore slightly modify the GMR model to fit it into a $p(4\times2)$ unit cell. A phase shift of adjacent wires could be

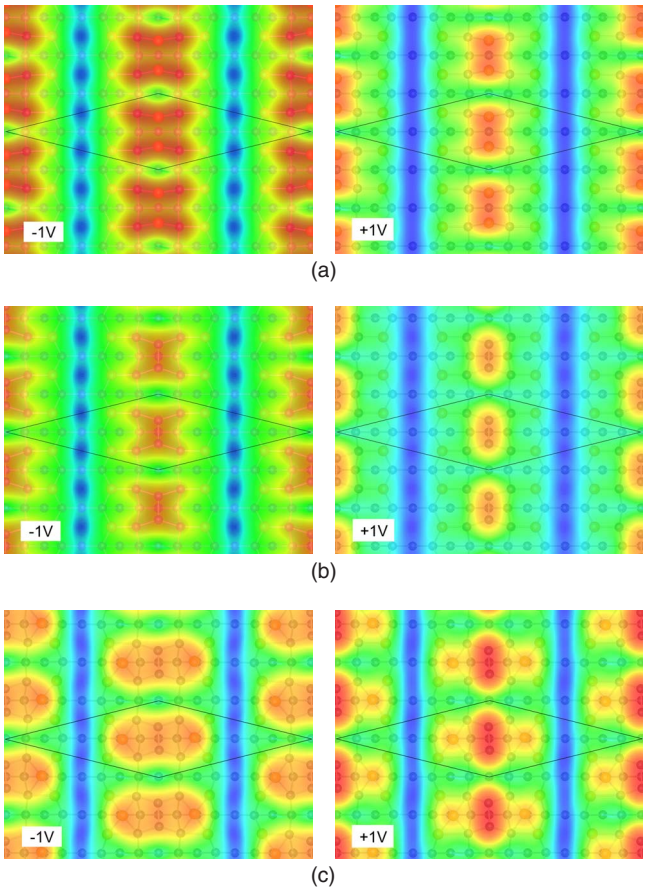

FIG. 7. (Color online) STM images for energetically favored bridging dimer models: (a) Au-BD, (b) Ge-BD, and (c) EBD. Left (right) panels are computed for occupied (empty) states. Bright/red regions describe protrusions while dark/blue areas indicate deep corrugations. The circles in the background refer to the atomic positions. Solid lines illustrate a $c(8\times2)$ unit cell.

used to create a $c(8\times2)$ reconstruction. Both unit cells cover the same area. The resulting atomic geometry is illustrated in Figs. 8(a) and 8(b). No trimerization of Au atoms is observed on the facets after the ionic relaxation, even if it was assumed in the starting configuration. Rather, the Au atoms occupy positions of the Ge bulk crystal, with extremely small deviations from the bulk positions of 0.02 Å in the nominal fifth Ge atomic layer and 0.28 Å in the third layer. The Au atoms are bonded via covalent bonds. The resulting Ge dimers on top of the ridge possess a bond length of 2.55 Å and a buckling angle of 17.8°. They are only somewhat shorter and less buckled compared to the clean surface. However, from the energetic point of view the GMR model is completely unfavorable (see Table III).

In order to improve the energetics upon the GMR model, we tested several rearrangements of Au atoms at the facets and additional exchange reactions. However, only the modified GMR model in Figs. 8(c) and 8(d) gave rise to a substantial improvement of the energetics of about 0.55 eV (GGA) or even 1.64 eV (LDA) (see Table III). Besides Au-Ge exchange at the facets, additional Ge dimers appear in the trenches with a bond length of 2.53 Å and a buckling angle of 18.7°. Compared to the original GMR model the depth of the trenches is reduced by the additional Ge dimers. Further, the high symmetry of the GMR ridges is disturbed by a twist of the top Ge dimers toward the wire direction by 15.0°. This distortion of the ridges can be increased even more by replacing Ge by Au atoms in the top dimers, i.e., Ge-Ge homodimers by Ge-Au heterodimers, which causes a significant reconstruction of the surface. The top dimer Au atoms move downward and form Au trimers at the facets [see Figs. 8(e) and 8(f)]. Consequently, the Ge atoms remaining on top of the ridges move toward each other, forming linear chains. We therefore call the result Au-trimer stabilized Ge ridge (ATSGR) model. For Au-rich preparation conditions its relative formation energy $\Delta\Omega_f$ [Eq. (3)] indicates stability with $\Delta\Omega_f=-0.44$ eV in DFT-GGA (compare Table III).

Despite the energetically less favorable geometry, the GMR model [Figs. 8(a) and 8(b)] gives rise to interesting constant-current STM images in Fig. 9(a), with a zigzag arrangement of current maxima. They qualitatively correspond with the ones measured by Schäfer *et al.*[15] for positive bias.

One possible explanation is the fact that the Fermi level in experiment is lower in energy due to a *p*-doping. The latter one could be due to the grains observed besides the wires in a distance of about 32 Å.[45] The MGMR model [Figs. 8(c) and 8(d)] shows features in the STM images which seem to be mixtures of those discussed for GMR and ATSGR. ATSGR yields almost linear features for both bias types while MGMR exhibits a pronounced zigzag behavior for negative voltages but less clear features for opposite bias sign.

Very interesting are the band structures of the GMR model [Fig. 10(a)] and the strongly modified ATSGR model [Fig. 10(b)]. The GMR model is metallic. The Fermi level crosses several bands. The most interesting metallic band is that with almost one-dimensional character in wire direction and a (filled) minimum near the center of the ΓX line at about −0.15 eV. The position of the minimum and its surface character seem to be in agreement with the ARPES measurements of Schäfer *et al.*[15] However, the band dispersion is too weak while the band filling (about 1/2) is too large. A stronger band dispersion would require a stronger interaction

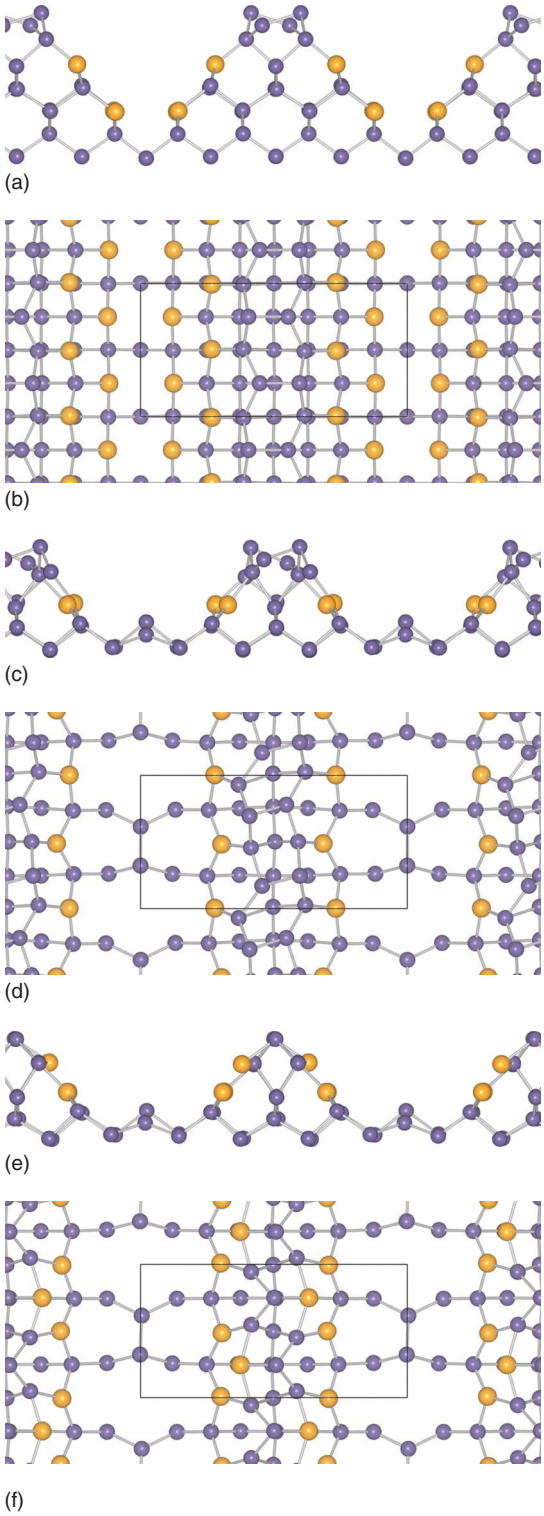

FIG. 8. (Color online) Side and top views of stick-and-ball models (relaxed geometries) for wires separated by deep trenches. (a) GMR, (b) MGMR, and (c) ATSGR models. The bright/orange (dark/blue) circles represent Au (Ge) atoms. A $p(4\times2)$ unit cell is indicated by solid lines. The Au coverage varies between $\Theta=0.50$ and 1.00.

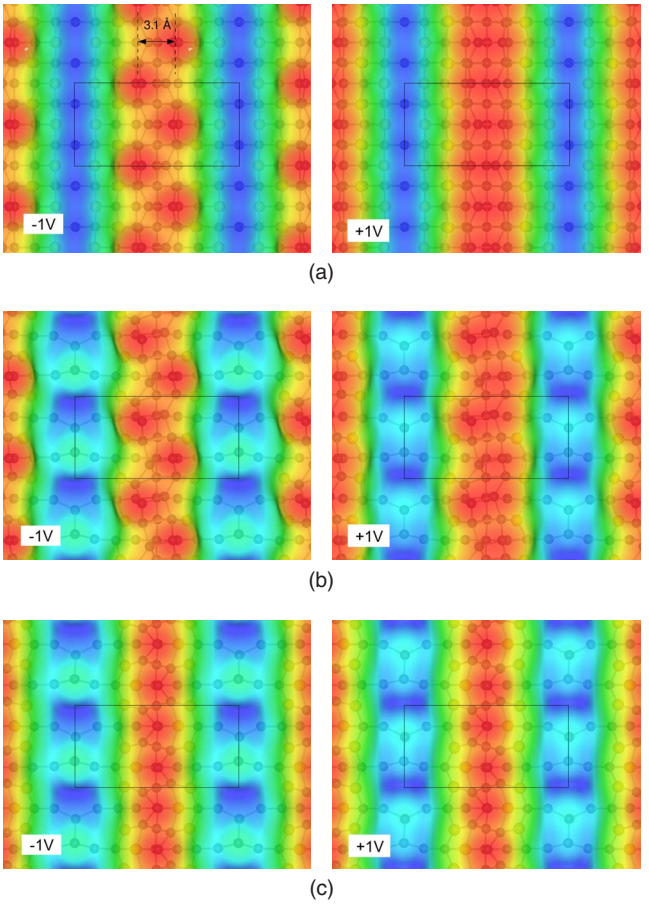

FIG. 9. (Color online) STM images for occupied states (left panels) and empty states (right panels) for (a) GMR, (b) MGMR, and (c) ATSGR models. The bright/red regions indicate wire ridges whereas dark/blue areas describe trenches between the wires. The underlying atomic geometry is also indicated.

of the ridge atoms. A possible reduction in the band filling may be explained by surface doping. In the case of the ATSGR model also metallic bands with almost 1D character occur along the direction of the nanowires ΓX. However, one is crossing the Fermi level at about 0.7ΓX while the rather flat one exhibits the minimum near 0.75ΓX. Both observations are not in agreement with the ARPES findings.[15]

VI. SUMMARY AND CONCLUSIONS

In summary, we have performed geometry, energy, and electronic-structure calculations within the density-functional theory using two different local or semilocal exchange-correlation functionals in order to explore the atomic geometry and stoichiometry of the gold-induced, quasi-one-dimensional nanowire arrays on top of a Ge(001) surface for several Au coverages. The explicit computations have been performed using the VASP package. In addition, for each interesting surface reconstruction we have calculated constant-current STM images for negative and positive tunnel bias since corresponding measurements have been published by three different experimental groups.

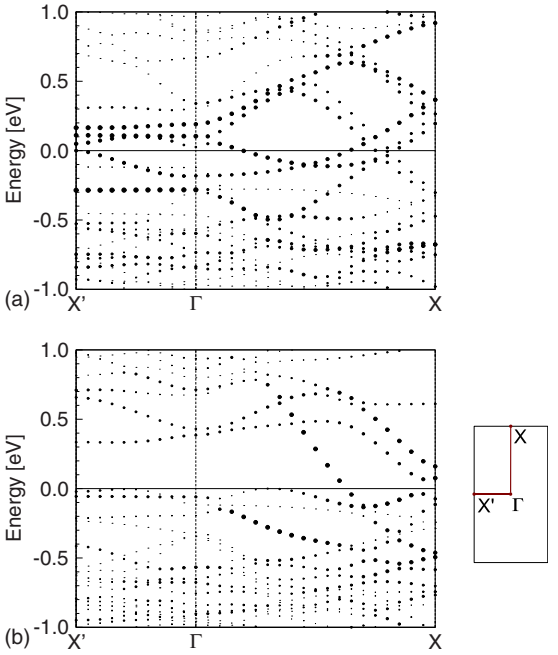

FIG. 10. (Color online) Band structure for the (a) GMR and (b) ATSGR models versus a direction ΓX along the wires and X′Γ perpendicular to the wires in the Brillouin zone of a $p(4\times2)$ surface. The size of the dots indicates the degree of localization at the surface. Consequently, the smallest dots represent states of the Ge substrate. The Fermi level is used as energy zero.

Altogether we have studied more than 150 candidates for surface models and their possible modifications. They can be classified in about four classes: (i) simple linear or zigzag gold chains on top or between Ge dimer rows of the clean Ge(001) surface that could be ruled out here due to their unfavorable energetics. (ii) Dimer-row models where dimer Ge-Ge homodimers are replaced by Au-Au dimers or Au-Ge heterodimers, which were found to give rise to a significant lowering of the surface formation energy, at least in DFT-GGA. Unfortunately, the resulting STM images cannot explain important experimental findings. (iii) Perpendicular dimers bridging two dimer rows together with the removal of every second dimer row of the clean Ge(001) surface were found to lead to very promising structural candidates from both points of view, the surface formation energy and the structural details seemingly observed in STM. Here, Au atoms stabilize {114} facets of the nanowires. However, these models cannot explain the differences in the STM images measured for filled and empty surface/nanowire states. (iv) The giant missing-row model follows the idea of relatively high nanowires with steep Au-stabilized facets (here {111}) and a wire ridge only of Ge atoms. It allows to describe rather pronounced nanowires and, most important, the differences between the STM images of filled and empty states can be uniquely explained by this model. However, the formation energy of the giant missing-row geometry is significantly too large to be the final explanation for the surface structure observed in experiments. Nevertheless, substantial modifications with rearrangements of the Ge ridges of the wires, the formation of Au trimers on the side facets, and additional Ge dimers in the trenches give rise to lower formation energies.

With only one-electron difference per noble-metal atom between Pt and Au, in contrast to the Pt/Ge(001) system the tetramer-dimer-chain model is unable to explain all the structural and spectroscopic details found for Au-induced wires on top of the Ge(001) surface. One reason is the favored bonding coordination of the Au atoms. Another one is the loss of the strong tendency of the Pt atoms to be incorporated in the surface in a more or less fourfold bonding configuration.

ACKNOWLEDGMENTS

The research leading to these results has received funding from the European Community, Seventh Framework Program (FP7/2007-2013) under grant agreement no 211956 and from the Deutsche Forschungsgemeinschaft (Projects Be 1346-20/1 and Scha 1510/2-1). We acknowledge CPU time from the supercomputer centers in Stuttgart and Munich.

[1] G. Grüner, *Density Waves in Solids* (Adison-Wesley, Reading, MA, 1994).
[2] J. M. Luttinger, J. Math. Phys. **4**, 1154 (1963).
[3] B. J. Kim, H. Koh, E. Rotenberg, S.-J. Oh, H. Eisaki, N. Motoyama, S. Uchida, T. Tohyama, S. Maekawa, Z.-X. Shen, and C. Kim, Nat. Phys. **2**, 397 (2006).
[4] R. Claessen, M. Sing, U. Schwingenschlögl, P. Blaha, M. Dressel, and C. S. Jacobsen, Phys. Rev. Lett. **88**, 096402 (2002).
[5] J. R. Ahn, P. G. Kang, K. D. Ryang, and H. W. Yeom, Phys. Rev. Lett. **95**, 196402 (2005).
[6] J. R. Ahn, H. W. Yeom, H. S. Yoon, and I.-W. Lyo, Phys. Rev. Lett. **91**, 196403 (2003).
[7] R. Losio, K. N. Altmann, A. Kirakosian, J.-L. Lin, D. Y. Petrovykh, and F. J. Himpsel, Phys. Rev. Lett. **86**, 4632 (2001).
[8] H. W. Yeom, S. Takeda, E. Rotenberg, I. Matsuda, K. Horikoshi, J. Schaefer, C. M. Lee, S. D. Kevan, T. Ohta, T. Nagao, and S. Hasegawa, Phys. Rev. Lett. **82**, 4898 (1999).
[9] J. Guo, G. Lee, and E. W. Plummer, Phys. Rev. Lett. **95**, 046102 (2005).
[10] C. González, J. Guo, J. Ortega, F. Flores, and H. H. Weitering, Phys. Rev. Lett. **102**, 115501 (2009).
[11] N. Oncel, A. van Houselt, J. Huijben, A.-S. Hallbäck, O. Gurlu, H. J. W. Zandvliet, and B. Poelsema, Phys. Rev. Lett. **95**, 116801 (2005).
[12] J. Schäfer, D. Schrupp, M. Preisinger, and R. Claessen, Phys. Rev. B **74**, 041404(R) (2006).
[13] A. A. Stekolnikov, F. Bechstedt, M. Wisniewski, J. Schäfer, and R. Claessen, Phys. Rev. Lett. **100**, 196101 (2008).
[14] J. Wang, M. Li, and E. I. Altman, Phys. Rev. B **70**, 233312 (2004).
[15] J. Schäfer, C. Blumenstein, S. Meyer, M. Wisniewski, and R. Claessen, Phys. Rev. Lett. **101**, 236802 (2008).
[16] K. Nakatsuji, R. Niikura, Y. Shibata, M. Yamada, T. Iimori, and F. Komori, Phys. Rev. B **80**, 081406(R) (2009).
[17] A. van Houselt, M. Fischer, B. Poelsema, and H. J. W. Zandvliet, Phys. Rev. B **78**, 233410 (2008).
[18] J.-H. Cho, D.-H. Oh, K. S. Kim, and L. Kleinman, J. Chem. Phys. **116**, 3800 (2002).
[19] X. López-Lozano, A. Krivosheeva, A. A. Stekolnikov, L. Meza-Montes, C. Noguez, J. Furthmüller, and F. Bechstedt, Phys. Rev. B **73**, 035430 (2006).
[20] C. González, F. Flores, and J. Ortega, Phys. Rev. Lett. **96**, 136101 (2006).
[21] A. A. Stekolnikov, K. Seino, F. Bechstedt, S. Wippermann, W. G. Schmidt, A. Calzolari, and M. Buongiorno Nardelli, Phys. Rev. Lett. **98**, 026105 (2007).
[22] S. Chandola, K. Hinrichs, M. Gensch, N. Esser, S. Wippermann, W. G. Schmidt, F. Bechstedt, K. Fleischer, and J. F. McGilp, Phys. Rev. Lett. **102**, 226805 (2009).
[23] D. Sánchez-Portal, J. D. Gale, A. García, and R. M. Martin, Phys. Rev. B **65**, 081401(R) (2002).
[24] A. A. Stekolnikov, J. Furthmüller, and F. Bechstedt, Phys. Rev. B **78**, 155434 (2008).
[25] G. Kresse and J. Furthmüller, Phys. Rev. B **54**, 11169 (1996).
[26] G. Kresse and J. Furthmüller, Comput. Mater. Sci. **6**, 15 (1996).
[27] G. Kresse and D. Joubert, Phys. Rev. B **59**, 1758 (1999).
[28] A. A. Stekolnikov, J. Furthmüller, and F. Bechstedt, Phys. Rev. B **65**, 115318 (2002).
[29] J. P. Perdew, in *Electronic Structure of Solids '91*, edited by P. Ziesche and H. Eschrig (Akademie-Verlag, Berlin, 1991), p. 11.
[30] J. P. Perdew and Y. Wang, Phys. Rev. B **45**, 13244 (1992).
[31] J. P. Perdew and A. Zunger, Phys. Rev. B **23**, 5048 (1981).
[32] H. J. Monkhorst and J. D. Pack, Phys. Rev. B **13**, 5188 (1976).
[33] C. Kittel, *Introduction to Solid State Physics*, 8th ed. (Wiley, New York, Chichester, 2004).
[34] P. Spiewak, K. Sueoka, J. Vanhellemont, K. Kurzydlowski, K. Mlynarczyk, P. Wabinski, and I. Romandic, Proceedings of the 24th International Conference on Defects in Semiconductors, 2007 [Physica B **401-402**, 205 (2007)].
[35] A. Nduwimana, X. G. Gong, and X. Q. Wang, Proceedings of Applied surface modeling: Experiment, Theory and Simulations, 2003 [Appl. Surf. Sci. **219**, 129 (2003)].
[36] J. P. Perdew, K. Burke, and M. Ernzerhof, Phys. Rev. Lett. **77**, 3865 (1996).
[37] J. Tersoff and D. R. Hamann, Phys. Rev. B **31**, 805 (1985).
[38] E. J. Snyder, E. A. Eklund, and R. Williams, Surf. Sci. **239**, L487 (1990).
[39] W. G. Aulbur, L. Jönsson, and J. W. Wilkins, in *Solid State Physics: Advances in Research and Applications* (Academic, San Diego, 2000), Vol. 54, p. 1.
[40] F. Bechstedt, *Principles of Surface Physics* (Springer-Verlag, Berlin, 2003).
[41] Z. Gai, R. G. Zhao, X. Li, and W. S. Yang, Phys. Rev. B **58**, 4572 (1998).
[42] A. A. Stekolnikov and F. Bechstedt, Phys. Rev. B **72**, 125326 (2005).
[43] L. Seehofer and R. Johnson, Surf. Sci. **318**, 21 (1994).
[44] P. B. Howes, C. Norris, M. S. Finney, E. Vlieg, and R. G. van Silfhout, Phys. Rev. B **48**, 1632 (1993).
[45] J. Schäfer, C. Blumenstein, S. Meyer, M. Wisniewski, and R. Claessen (unpublished).